Comparative parallel analysis of RNA ends identifies mRNA substrates of a tRNA splicing endonuclease-initiated mRNA decay pathway

Jennifer E. Hurtig[a], Michelle A. Steiger[a,b], Vinay K. Nagarajan[c], Tao Li[d], Ti-Chun Chao[d], Kuang-Lei Tsai[d], and Ambro van Hoof[a,1]

[a]Microbiology and Molecular Genetics, University of Texas Health Science Center, Houston, TX 77030; [b]Department of Chemistry and Biochemistry, University of St. Thomas, Houston, TX 77006; [c]Delaware Biotechnology Institute, University of Delaware, Newark, DE 19713; and [d]Biochemistry and Molecular Biology, University of Texas Health Science Center, Houston, TX 77030

Edited by Roy Parker, University of Colorado Boulder, Boulder, CO, and approved January 25, 2021 (received for review September 29, 2020)

Eukaryotes share a conserved messenger RNA (mRNA) decay pathway in which bulk mRNA is degraded by exoribonucleases. In addition, it has become clear that more specialized mRNA decay pathways are initiated by endonucleolytic cleavage at particular sites. The transfer RNA (tRNA) splicing endonuclease (TSEN) has been studied for its ability to remove introns from pre-tRNAs. More recently it has been shown that single amino acid mutations in TSEN cause pontocerebellar hypoplasia. Other recent studies indicate that TSEN has other functions, but the nature of these functions has remained obscure. Here we show that yeast TSEN cleaves a specific subset of mRNAs that encode mitochondrial proteins, and that the cleavage sites are in part determined by their sequence. This provides an explanation for the counterintuitive mitochondrial localization of yeast TSEN. To identify these mRNA target sites, we developed a "comPARE" (comparative parallel analysis of RNA ends) bioinformatic approach that should be easily implemented and widely applicable to the study of endoribonucleases. The similarity of tRNA endonuclease-initiated decay to regulated IRE1-dependent decay of mRNA suggests that mRNA specificity by colocalization may be an important determinant for the degradation of localized mRNAs in a variety of eukaryotic cells.

mRNA degradation | tRNA splicing | endonuclease

RNA degradation is a complex process that requires multiple ribonucleases in every domain of life. These multiple ribonucleases act sequentially on individual messenger RNA (mRNA) molecules to completely degrade them. Diverse eukaryotes share a conserved cytoplasmic pathway for the degradation of most cellular mRNAs. First, the poly(A) tail is removed by Ccr4/Not and Pan2/3 exoribonuclease complexes. This deadenylation can be followed either by removal of the cap structure by Dcp2 and 5′ to 3′ digestion by the exoribonuclease Xrn1, or by 3′ to 5′ digestion by the RNA exosome. In this pathway, removal of the 5′ cap and 3′ poly(A) tail are rate-limiting and these structures protect mRNAs from degradation by exonucleases. The contributions of each of these ribonucleases to mRNA degradation have been well characterized (1–7) and Ccr4/Not, Pan2/3, Dcp2, Xrn1, and the RNA exosome are conserved throughout eukaryotes.

Along with digestion from either end, mRNA degradation can be initiated by a variety of endonucleases. These endonuclease-initiated pathways have been less well characterized, may be less extensively conserved, and generally target only a subset of mRNAs. The endonucleases generally cleave at a small number of specific sites within an mRNA target and produce two products: One with a 5′ cap, but no 3′ poly(A) tail and one that is uncapped but has a poly(A) tail. Because both products lack one protective end, they are then further degraded by the RNA exosome and Xrn1.

One prominent example of endonuclease-initiated mRNA decay is RNA interference initiated by the RNA-induced silencing complex (RISC). The core of RISC, conserved in animals, fungi, and plants, consists of a small RNA and a catalytic Argonaut subunit. RISC uses the small RNA to recognize complementary mRNAs and cleave them (8). These cleavage products are degraded by Xrn1 and the RNA exosome (9–12). A second example of endonuclease-initiated mRNA decay is cleavage of mRNAs that contain premature stop codons in Metazoa by the SMG6 endonuclease (13, 14), followed by XRN1 and RNA exosome-mediated degradation of the cleavage products (14). A third example of endonuclease-initiated mRNA decay is the regulated IRE1-dependent decay (RIDD) pathway. The endoribonuclease IRE1 is activated when unfolded proteins accumulate in the endoplasmic reticulum (ER), and functions in two ways to restore homeostasis to the ER. First, IRE1 cleaves two sites within the mammalian *XBP-1* mRNA (or the yeast *HAC1* mRNA) to initiate a noncanonical splicing event (15, 16). The resulting *XBP-1* (or *HAC1*) mRNA encodes a transcription factor that activates genes integral to protein folding in the ER (17). The second function of IRE1 is to cleave a number of mRNAs that encode ER-localized proteins (18–21), which functions to reduce the import of newly translated proteins into the ER and therefore the need for protein folding in the ER. Cleavage of mRNAs by IRE1 is also followed by degradation by XRN1 and the RNA exosome (21). Together, the increased folding capacity mediated

Significance

The transfer RNA (tRNA) splicing endonuclease (TSEN) has a well-known role in cleaving pre-tRNAs to remove introns, but has other uncharacterized functions. Here we show that yeast TSEN cleaves several mRNAs that encode mitochondrial proteins, and that the cleavage sites are in part determined by their sequence. This provides an explanation for the counterintuitive mitochondrial localization of yeast TSEN. Human patients that inherit mutations in TSEN are born with pontocerebellar hypoplasia, which may be because of a defect in the mRNA cleavage functions of TSEN. The similarity of this TSEN-initiated decay pathway to other mRNA decay pathways suggests that mRNA specificity by colocalization may be an important determinant for the degradation of localized mRNAs in a variety of eukaryotic cells.

Author contributions: J.E.H., M.A.S., V.K.N., and A.v.H. designed research; J.E.H., M.A.S., V.K.N., T.L., T.-C.C., and K.-L.T. performed research; J.E.H., T.L., T.-C.C., and K.-L.T. contributed new reagents/analytic tools; J.E.H., M.A.S., and A.v.H. analyzed data; and J.E.H., M.A.S., V.K.N., T.L., T.-C.C., K.-L.T., and A.v.H. wrote the paper.

The authors declare no competing interest.

This article is a PNAS Direct Submission.

[1]To whom correspondence may be addressed. Email: ambro.van.hoof@uth.tmc.edu.

This article contains supporting information online at https://www.pnas.org/lookup/suppl/doi:10.1073/pnas.2020429118/-/DCSupplemental.

Published March 1, 2021.

by *XBP-1* splicing and reduced need for folding mediated by RIDD restore homeostasis to the ER. A fourth example of an endonuclease that initiates mRNA decay is the transfer RNA (tRNA) splicing endonuclease (TSEN), for which we propose the name TED (tRNA endonuclease-initiated mRNA decay). The canonical function of TSEN is to cleave pre-tRNAs to initiate the nonspliceosomal splicing of pre-tRNA (22–24). Recently, TSEN was shown to have a second function; it cleaves the yeast *CBP1* mRNA and the resulting cleavage products are degraded by Xrn1 and the RNA exosome (25). Genetic evidence suggests that TSEN has a third function, but the nature of this function is unknown (26, 27).

In each of these cases, endonuclease-initiated mRNA decay appears to target a subset of mRNAs, but which mRNAs are targeted and how they are recognized is incompletely understood. One factor that contributes to mRNA specificity of both RIDD and TED is colocalization of the mRNAs and endonucleases. The Ire1 endonuclease of the RIDD pathway is localized on the outside of the ER, facing the cytoplasm (28–30). Similarly, TSEN of the TED pathway is localized on the outside of the mitochondria, facing the cytoplasm (31, 32). Both pathways target mRNAs that are localized to the outside of these same organelles, and the localization of the target mRNAs is at least in part dependent on the cotranslational recognition of the signal sequence/transit peptide of the nascent protein (21, 25). However, not all mRNAs that are localized to the ER or mitochondrial surface are targeted and not all sites within an mRNA are cleaved equally, indicating that other features contribute to the determination of which phosphodiester bonds get cleaved. RIDD, for example, also shows specificity for sequence and structure (33). Whether TED is also sequence- and structure-dependent has not been extensively studied. A target structure for *CBP1* was proposed (25), but this structure does not appear to be conserved in other *Saccharomyces* species and its importance has not been rigorously tested by compensatory mutations. Our understanding of TED specificity and physiological function is limited, at least in part because only one substrate (*CBP1*) is known.

Parallel analysis of RNA ends (PARE) is a useful tool for finding endonuclease targets (34–37). This method uses T4 RNA ligase to ligate a linker onto the 5′ ends of polyadenylated RNAs with a free 5′ monophosphate. The linker can then be used for library preparation and deep sequencing, which maps the exact 5′ monophosphate end of the RNA. Intact mRNAs normally have a ^{7m}GpppN cap structure and are therefore not substrates for this ligation. Moreover, any 5′ monophosphate mRNAs that arise by either decapping or endonuclease digestion are rapidly degraded by Xrn1. Here we use PARE to identify 5′ monophosphate mRNAs present in *xrn1Δ* but that disappear if TSEN is inactivated. The *xrn1Δ* allows the detection of 5′ monophosphate intermediates that are normally very transient. Identification of endonuclease sites has been limited by a lack of easily accessible bioinformatics tools. Here we develop a comparative PARE pipeline (comPARE) that can be easily implemented on a public Galaxy server (usegalaxy.org) and does not require any coding. This should make the comPARE analysis method readily accessible to RNA biologists with limited bioinformatics expertise. With this method, we were able to identify novel TED targets, and show that TED has sequence specificity.

Results

PARE Sensitively Identifies Known TSEN Cleavage Sites in Endogenous *CBP1*. When RNA is cleaved by an endonuclease or decapped, a 5′ monophosphate is formed on the 3′ cleavage product. Some endonucleases directly produce 5′ monophosphates, while others produce 5′ hydroxyl ends that are subsequently phosphorylated by a polynucleotide kinase. Xrn1 requires a 5′ monophosphate for further degradation. PARE takes advantage of this end to ligate an adaptor to cleaved mRNAs (Fig. 1*A*) (34). After ligation, the PARE adaptor is used for next-generation sequencing (NGS) library generation, which is then sequenced from the adaptor end. Therefore, the first nucleotide in the NGS read precisely corresponds to the first nucleotide in the 5′ monophosphate RNA. We initially attempted to use PARE to investigate the endonuclease domain of the RNA exosome (38–40). Many targets of the exonuclease activity of the RNA exosome are known but targets of the highly conserved endonuclease domain have remained elusive. To investigate targets of the RNA exosome endonuclease activity, we used PARE on *xrn1Δ* and *xrn1Δ rat1-1* yeast strains. Xrn1 and Rat1 are the major processive 5′ exoribonucleases in the cytoplasm and nucleus, respectively (7). Thus, these mutations are expected to stabilize most endoribonuclease cleavage products.

Previous PARE studies have used *xrn1* single mutants or depletion, and we reasoned that adding *rat1-1* would expand the degradome studies to nuclear events. Other 5′ exonucleases (e.g., Dxo1, Rai1, Rrp17, Ysh1) have been found to play minor roles in RNA degradation and do not interfere with PARE (41–44). We also included *xrn1Δ rrp44-endo*$^{-}$ and *xrn1Δ rat1-1 rrp44-endo*$^{-}$ strains that additionally lack the endonuclease activity of the

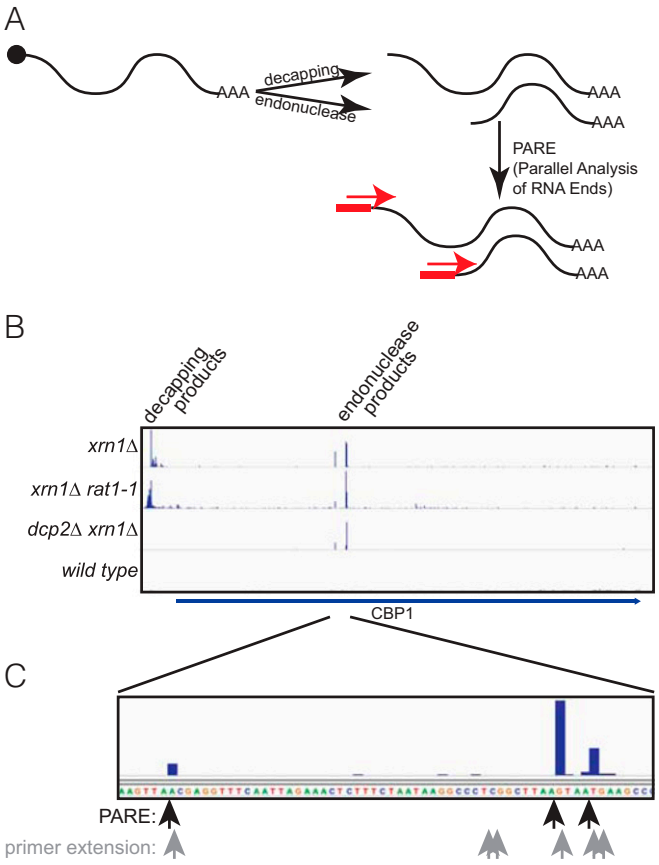

Fig. 1. PARE detects previously identified cleavage sites within the *CBP1* mRNA. (*A*) The PARE method is outlined. A linker (red rectangle) is ligated to 5′ monophosphates on polyadenylated RNA that result from decapping or endonucleolytic cleavage. Capped (Black circle) RNA is resistant to ligation. This linker is then used in NGS sequencing, resulting in a sequence read (red arrow) that precisely starts at the first nucleotide of the 5′ monophosphorylated RNA. (*B*) Initial PARE analysis for *xrn1Δ* and *xrn1Δ rat1-1* strains (top two panels) and published data from *dcp2Δ xrn1Δ* and wild-type strains (bottom two panels). Despite differences in the methods, similar endonuclease peaks were identified in all the strains that lacked Xrn1, showing the robustness of the method. (*C*) Zoomed-in view of the *xrn1Δ* data from *B*. The major PARE peaks are highlighted (black arrows), as is the previous mapping of cleavage sites by primer extension (gray arrows).

RNA exosome. Each of these strains was used in biological duplicates. Thus, the cytoplasmic degradome was sequenced in four replicates as has been done previously (35). The four replicates of *xrn1Δ rat1-1* (with and without *rrp44-endo*$^{-}$) represent the first characterization of the nuclear degradome of *Saccharomyces cerevisiae*. Unfortunately, we were unable to identify any novel targets of the RNA exosome endonuclease domain, perhaps because it does not cleave any particular site at high frequency. Similarly, our previous microarray analysis was also unable to determine genes that were differentially expressed in the absence of the endoribonuclease activity (45).

While analyzing our PARE data we did observe prominent peaks for several known endonuclease cleavage sites, including peaks in *CBP1*, the only known target for TED (Fig. 1*B*) (25). These *CBP1* peaks were highly reproducible in the eight PARE datasets. We observed the same peaks in *dcp2Δ xrn1Δ* PARE data previously published by the Parker laboratory (35), but not the wild-type control strain from that study (Fig. 1*B*). Thus, these peaks do not reflect decapped mRNAs. In contrast, the peaks just upstream of the *CBP1* ORF were absent in the *dcp2Δ xrn1Δ* samples and thus reflect decapped mRNAs.

Five TSEN cleavage sites in *CBP1* have previously been identified by primer extension analysis (25). The PARE peaks we identified were near, but not exact matches to the primer extension sites (Fig. 1*C*). This is at least in part because the previous studies used an overexpressed *CBP1*. When we repeated the PARE analysis upon overexpression of *CBP1*, we also saw slightly different peaks. Specifically, while both endogenous and overexpressed *CBP1* were cleaved after nucleotides 669, 714, and 719 of the coding region, the 714 site was more prominent in endogenous *CBP1* while the 719 site was more prominent after *CBP1* overexpression (*SI Appendix*, Fig. S1). Overexpression also resulted in prominent PARE signals at nucleotides 720 and 670 of *CBP1* that were not seen for the endogenous mRNA. These observations confirm that PARE can map endonuclease cleavage sites while avoiding the need to overexpress target RNAs.

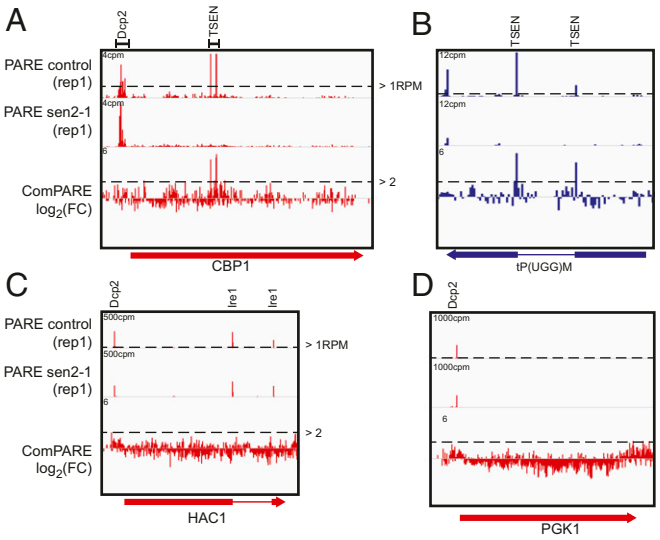

Fig. 2. comPARE identifies TSEN-dependent cleavage sites. (*A*) Cleavage sites in *CBP1* detected in *xrn1Δ* (*Top*) are strongly reduced in *sen2-ts xrn1Δ* (*Middle*), confirming that TSEN is required for this cleavage. Note that the PARE signals for TSEN products is off the *y* axis scale. A scale of 0 to 4 was used to visualize the decapping products. The actual height of the TSEN PARE peaks is listed in *SI Appendix*, Table S1. (*B*) The cleavage sites in the proline pre-tRNA *tP(UGG)M* detected in *xrn1Δ* are strongly reduced in *sen2-ts xrn1Δ*, confirming that TSEN is required for this cleavage. (*C*) The cleavage sites in *HAC1* are similarly detected in *xrn1Δ* and *sen2-ts xrn1Δ*, confirming that TSEN is not required for this Ire1-mediated cleavage. (*D*) No significant cleavage sites were detected in the *PGK1* mRNA. This mRNA is normally degraded by Dcp2-mediated decapping and Xrn1-mediated 5′ to 3′ degradation, but in the *xrn1Δ* strains used here is known to be degraded by the 3′ exoribonuclease activity of the RNA exosome.

comPARE: A Quantitative Measure of the Dependence of a PARE Site on a Specific Endonuclease. To determine whether the peaks we observed in *CBP1* were indeed produced by TSEN, we generated additional PARE data. We grew an *xrn1Δ sen2-ts* strain [carrying a temperature sensitive mutation in TSEN (46)] and an *xrn1Δ* strain in duplicate at room temperature, incubated all four cultures at 37 °C for 1 h to inactivate TSEN, and performed PARE. As shown in Fig. 2*A* and consistent with previous data (25) (Fig. 1), the prominent peaks in the *CBP1* ORF were again detected in the *xrn1Δ* PARE data (Fig. 2 *A*, *Top*), but not in the *xrn1Δ sen2-ts* datasets (Fig. 2 *A*, *Middle*). In contrast, the peaks corresponding to decapped *CBP1* mRNA were present in all four datasets. This confirms that TSEN is required for the cleavage of endogenous *CBP1* (25).

To develop a bioinformatic approach to identify additional TSEN cleavage sites that is simple to implement, we turned to tools available on a public Galaxy server (usegalaxy.org). Briefly, we first used the Bamcoverage tool to count the number of reads starting at every position in the genome (i.e., at single-nucleotide resolution, with no binning). For each sample, this generated a file containing the counts of read 5′ ends for each strand of the genome, normalized to total reads mapped (essentially counts per million at single-nucleotide resolution), which we refer to as the PARE score. The PARE scores for each nucleotide in *CBP1* are plotted in the *Top* and *Middle* panels of Fig. 2*A*. Second, we used bigwigCompare to divide the number of reads in an *xrn1Δ* sample by the number of reads in the matching *xrn1Δ sen2-ts* sample. Essentially, this generated a $\log_2$(fold-change) at single-nucleotide resolution, which we will refer to as the comPARE score. This comPARE score is plotted along the *CBP1* gene in the *Bottom* panel of Fig. 2*A*. As shown in this panel, the TSEN-dependent cleavage sites in *CBP1* have high comPARE scores. In contrast, the decapping products received a low comPARE score, indicating that they are not affected by the *sen2* mutation. Both Bamcoverage and bigwigCompare output bigwig files which can be visualized directly in IGV (https://software.broadinstitute.org/software/igv/download). Finally, we used the Merge BedGraph files tool to generate one table of 24 million rows (representing nucleotide resolution on both strands of the 12-MB genome) and four columns of PARE scores (from the duplicate *xrn1Δ* and *xrn1Δ sen2-ts* samples) and two columns of comPARE scores.

To assess the viability of comPARE to identify TSEN cleavage sites, we examined the PARE and comPARE scores for known cleavage sites between *xrn1Δ* and *xrn1Δ sen2-ts* strains (Fig. 2). We filtered the data for positions where both *xrn1Δ* PARE scores were larger than 1 (indicated by the dashed line in Fig. 2). This filters out low-level noise and keeps positions that have more than 1 read per million mapped reads. The *CBP1* cleavage sites exceeded this threshold (Fig. 2*A*). Although PARE enriches for poly(A)+ RNA, some of the known TSEN sites in tRNA also exceeded this PARE > 1 threshold (Fig. 2*B*). As an example of sites from another endonuclease, the Ire1 cleavage sites in the *HAC1* mRNA also exceeded PARE > 1, even though our samples were not specifically treated to activate Ire1 (Fig. 2*C*). In contrast, in an *xrn1Δ* strain the *PGK1* mRNA is degraded by the 3′ exoribonuclease activity of the RNA exosome (47, 48) and reassuringly the *PGK1* ORF did not contain any PARE > 1 peaks. Only the *PGK1* decapping peak upstream of the ORF was detected. Thus, the PARE > 1 filter appears suitable to reduce low level background noise and reduces the data from 24 million rows to ∼100,000 rows.

To distinguish TSEN products from those produced by decapping and other endonucleases, we filtered on a comPARE score >2 or <−2 (or a fourfold change in signal upon TSEN

GENETICS

inactivation). A total of 465 positions exceeded this threshold, of which 464 showed a decrease in signal in *sen2-ts*. The only increased signal barely exceeded the comPARE <−2 threshold (Fig. 3*A*). The known TSEN sites in *CBP1* and tRNAs exceeded that threshold, but the Ire1 sites in *HAC1* and the decapping sites in *CBP1*, *HAC1*, and *PGK1* did not, reflecting that these sites are not TSEN cleavage sites (*Bottom* panels in Fig. 2). Many of the top scoring positions were at pre-tRNA splice sites or within ORFs. Limiting the signals to ones that occur at pre-tRNA splice sites or within ORFs reduced the number of positions to 180, all of which were down in the *sen2* mutant (Fig. 3*B*). Several of the high-scoring ORFs (including *CBP1* and *PKP2*) contained several cleavage positions (Fig. 3*B*). The highest scoring position was one of the known cleavage sites in *CBP1*. Taken together, these results indicate that PARE can reliably identify endonuclease cleavage sites in mRNAs (and pre-tRNAs) expressed at their endogenous level, and that comPARE can identify exact cleavage sites of specific endonucleases such as TSEN.

comPARE Identifies a Small Subset of mRNAs that Encode Mitochondrial Proteins as TED Targets. The initial comPARE analysis identified 19 sites in the genome with a comPARE > 4 in both replicates. Four cleavage events in *CBP1* (Fig. 2*A*) had the 1st, 4th, 10th, and 16th highest comPARE score (average comPARE scores 7.3, 5.7, 5.1, and 4.5, respectively). Four pre-tRNA cleavage sites also had average comPARE > 4. We were surprised to detect any tRNA substrates as PARE is designed to identify polyadenylated degradation intermediates that are degraded by Xrn1. The released tRNA exons and introns are not expected to be polyadenylated, the released exons are not stabilized by *xrn1*Δ but instead are rapidly ligated by Trl1 (22, 49, 50), and the released exons and introns are too small for the size-selection step in

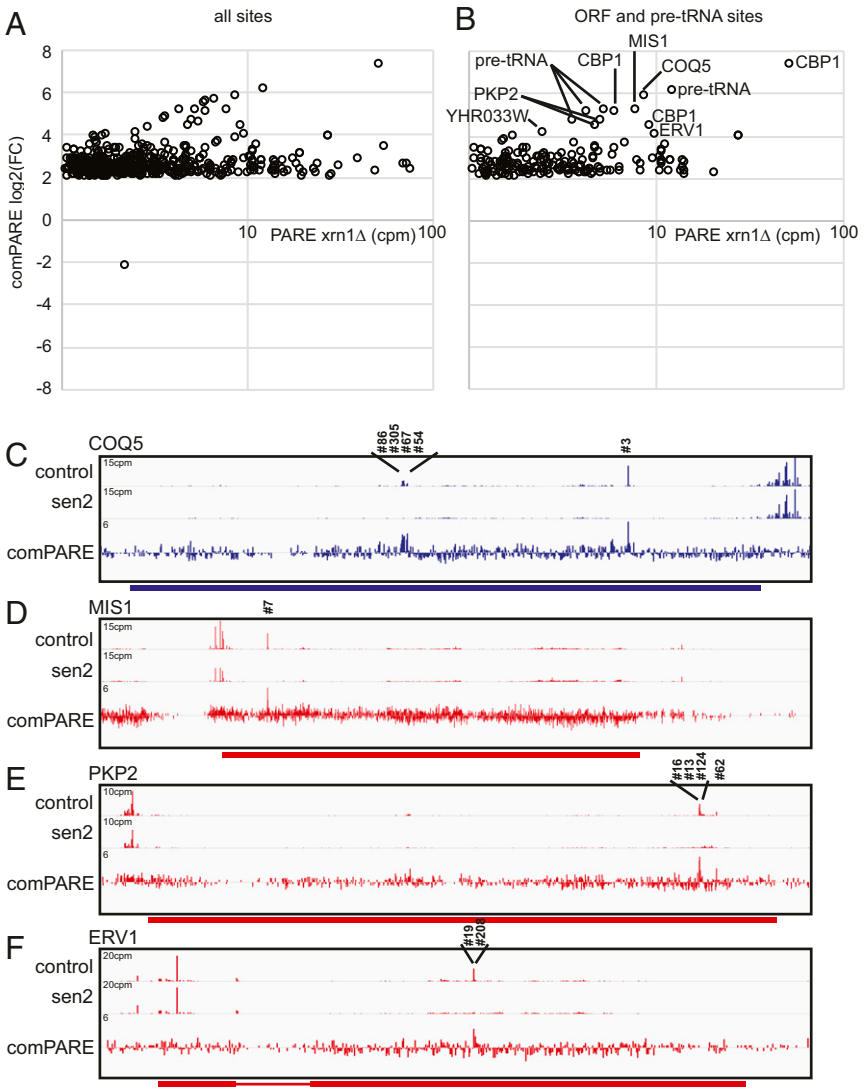

Fig. 3. comPARE reveals previously unknown TSEN-dependent cleavage sites in mRNAs. (*A*) All 24 million potential sites in the genome were filtered for sites that have PARE score >1 in two biological *xrn1*Δreplicates, and a comPARE score either >2 or <−2. This highlights sites that are detectable in *xrn1Δ*, but either disappear (comPARE >2) or become more prominent (comPARE <-2) in *xrn1Δ sen2-ts*. Plotted is the average PARE score (*x* axis) of two biological replicates against the average comPARE score (*y* axis) of two biological replicates. Thus, data points toward the right end of the graph reflect 5′ monophosphate RNAs that are prominent in *xrn1Δ*, while data toward the top reflect 5′ monophosphate RNAs that are much less prominent in *xrn1Δ sen2-ts*. (*B*) As in *A*, but only data points within ORFs or at pre-tRNA splice sites are included. (*C*) TSEN dependent-cleavages in *COQ5* are detected in *xrn1Δ* (*Top*), but not in the *xrn1Δ sen2-ts* (*Middle*), resulting in their high comPARE score (*Bottom*). The numbers above each peak indicates their rank in order of comPARE score. For example, the third highest score is for a site in *COQ5*, as are sites ranked 54, 67, 86, and 305. (*D–F*) As in *C*, except that results for *MIS1*, *PKP2*, and *ERV1* are shown. *C–F* show results from one biological replicate. The other replicate showed very similar results as shown in Fig. 7 and *SI Appendix*, Fig. S3.

library preparation. Nevertheless, *CBP1* and pre-tRNAs accounted for 8 of the top 19 comPARE hits. When examining the read maps of these comPARE hits, peaks are clearly visible in the control and disappear in *sen2-ts*, validating our comPARE scores. The other 11 hits included 6 sites in 5 other ORFs that encode mitochondrial proteins (Fig. 3 *C–F*) [*COQ5*, *MIS1, PKP2*, *ERV1,* and *YHR033W* (51–53)], and 5 intergenic regions. The enrichment for mRNAs localized to the mitochondria is expected as the TSEN complex localizes to the mitochondrial membrane in yeast and this localization has been shown to be required for the other unknown essential function of TSEN (26, 54).

To confirm that TSEN is directly cleaving these newly identified mRNAs we generated in vitro-transcribed RNAs that span from ∼60 nt upstream of the PARE site to ∼60 nt downstream and incubated those RNAs with purified recombinant yeast TSEN. As shown in Fig. 4, each of the substrates were cleaved by TSEN and produced major products of the expected size (indicated with an asterisk in Fig. 4). Notably, pre-tRNA–Phe [specifically tF(GAA)F] was cleaved more efficiently than the candidate mRNA sites. This preference is expected as in vivo TSEN cleaves pre-tRNA to initiate its function, while the mature mRNA is cleaved/degraded slower to allow the functional protein to be translated before the mRNA is cleaved. When compared to each other, the mRNAs were cleaved with different efficiencies, but all were cleaved better than a control mRNA fragment (Fig. 4). *COQ5* was cleaved least efficiently, perhaps because not all sequence elements required for efficient cleavage are within 60 nt of the main cleavage site (*Discussion*).

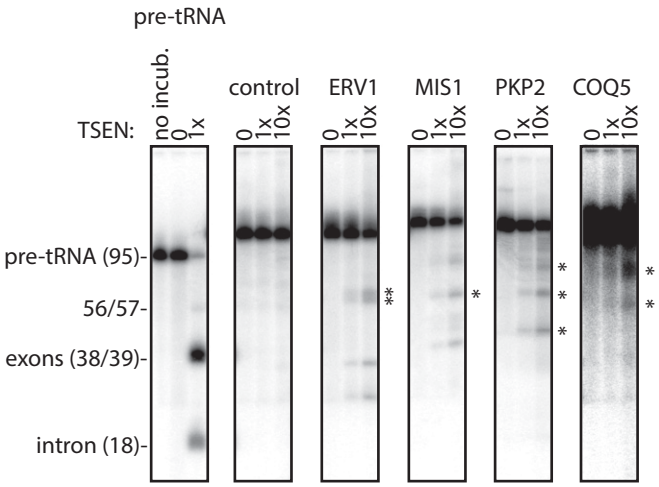

Substrate	size	expected products
pre-tRNA	95	39 + 38 + 18
control	128	N/A
ERV1	122	62 + 60
MIS1	123	62 + 61
PKP2	137	75 + 62 (+40 + 35)
COQ5	129	73 + 56

Fig. 4. Novel TSEN-mediated cleavage sites identified from comPARE are cleaved by recombinant TSEN in vitro. RNAs from ∼60 nt upstream of the novel TSEN sites to ∼60 nt downstream were incubated in vitro with purified yeast TSEN, expressed in a baculovirus system. As a positive control (*Left*) pre-tRNA–Phe [specifically tF(GAA)F] was incubated either in the presence (third lane) or absence (second lane) of recombinant TSEN, or analyzed without any incubation (first lane). As a negative control, a distal piece of the *CBP1* mRNA was used (second panel). For panels two to six, the indicated RNA was incubated without recombinant TSEN, with a relatively low concentration of TSEN or a 10-fold higher concentration of TSEN. Products of the expected size are indicated with an asterisk (*). Additional ERV1 products of 35 and 20 nt that are not marked are discussed in the discussion. Each panel is from a gel that also included a pre-tRNA–Phe reaction which provided size markers to identify the expected products. The *COQ5* panel is exposed darker than the other panels to visualize the faint product bands. The table below the gels lists the size of the substrates and expected products. PARE detects two sites in *PKP2*. A single cleavage of the major *PKP2* site results in 75- and 62-nt products, while a second cleavage produces 40- and 35-nt products from the 75-nt fragment, which are indicated in parentheses.

TSEN Cleaves mRNAs after Specific As. Upon identification of these novel targets, we sought to identify any similarity between them in terms of sequence or secondary structure that TSEN could use to recognize its substrates. TSEN has been hypothesized to recognize the overall fold of tRNA (55–57), and a stem loop structure within *CBP1* (25). In addition, TSEN in Archaea and eukaryotes recognizes an ∼4-bp helix to identify its tRNA targets (56, 58). However, secondary structure prediction revealed no obvious structural similarities between the newly identified targets, *CBP1*, and tRNAs. Secondary structure prediction remains a challenging problem, and future studies are needed to determine whether these TSEN substrates share a similar structure that TSEN recognizes.

Next, we examined if there was a shared sequence or motif around the sites TSEN cleaves. This revealed a motif shared between the mRNA cleavage sites (Fig. 5*A*). This motif includes a strong enrichment for an A immediately preceding the cleavage site (the −1 position). There is also a preference for an A in position −2 as well as for G or U at −3. Notably, these preferences are all upstream of the cleavage site and thus not in the PARE sequencing read that starts at +1. As such, these preferences cannot be explained by preferences of T4 RNA ligase or some other aspect of NGS library preparation or sequencing, but must reflect TSEN specificity. We tested the importance of this motif by mutating the −1A of *CBP1* to C. Specifically, we changed the −1As for all three prominent PARE peaks in endogenous *CBP1* to C, generating a *CBP1-3AC* mutant, and analyzed the effects both in vivo and in vitro.

To analyze the requirement for −1A in vivo, we expressed either wild-type *CBP1* or *CBP1-3AC* from a GAL promoter in an *xrn1Δ* strain. *xrn1Δ* stabilizes the 3′ cleavage product to detectable levels, as described previously (25). Northern blot analysis revealed that the *CBP1-3AC* mutant reproducibly accumulated less of the cleavage fragment (Fig. 5*B*). To quantitate the effect on cleavage we normalized cleaved *CBP1* levels to that of full-length *CBP1* mRNA. In four biological replicates, cleavage of *CBP1-3AC* was reduce to an average of 0.33 (±0.16 SD) relative to the normal *CBP1* mRNA (Fig. 5*C*). Similarly, mutations that inactivate the cytoplasmic exosome, such as *ski7Δ*, stabilize the 3′ cleavage product to detectable levels, as described previously (25). The abundance of this fragment was reduced to 0.41 (±0.09) for the *CBP1-3AC* mRNA (Fig. 5*D*). A one-sample *t* test indicates that these reductions in both cleavage products are statistically significant ($P < 0.005$ for each). Note that the *CBP1-3AC* allele has the −1 nucleotide for the three most prominent PARE sites mutated, but in the context of the overexpression construct used, additional PARE peaks are detected (*SI Appendix*, Fig. S1). Therefore, the cleavage product that remains in the *CBP1-3AC* mutant likely includes cleavage products only seen in the overexpressed *CBP1*. These results indicate that TSEN recognizes an A at −1 for efficient cleavage in vivo.

To analyze the requirement for A at −1 in vitro, we used a 75-nt substrate RNA that was previously shown to be cleaved by TSEN partially purified from yeast (25). When we incubated the same RNA with recombinant TSEN it was cleaved at the expected sites (Fig. 5*E* and *SI Appendix*, Fig. S2). PARE analysis indicates that *CBP1* is cleaved in vivo after nucleotides 669, 715, and 719, with the latter cleaved less efficiently. We thus expected major fragments of 46, 18, and 11 nt (and perhaps minor products of

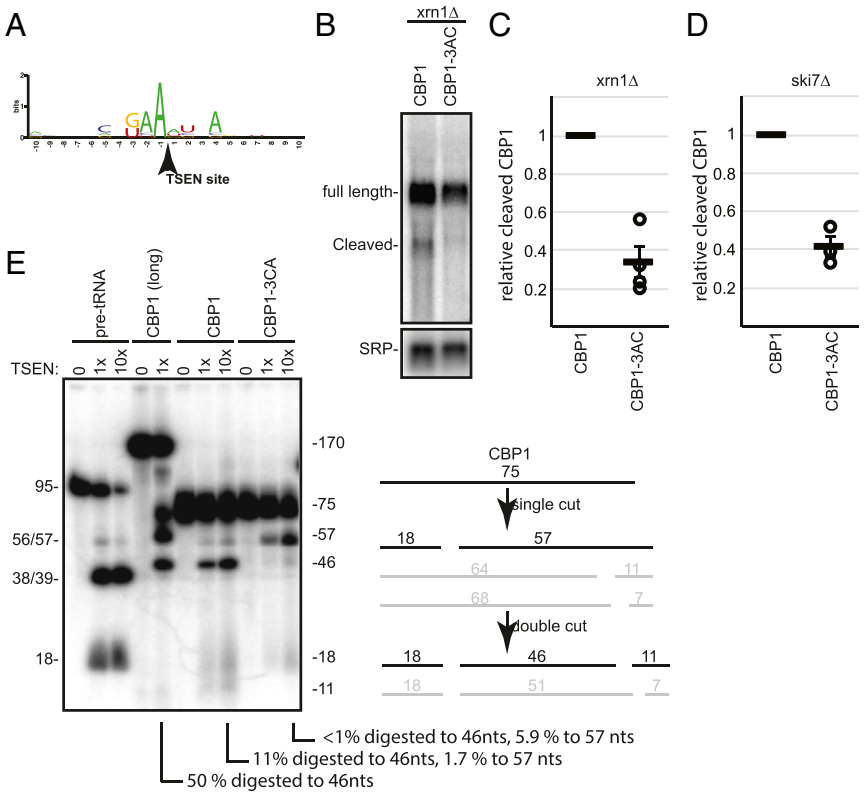

Fig. 5. TSEN recognizes an A residue immediately 5′ of the cleavage site. (*A*) Shown is a sequence logo of the top cleavage sites from Fig. 3, indicating that TSEN has some sequence specificity. (*B*) Northern blot analysis of wild-type *CBP1* or a mutant with the −1A nucleotide for the three most prominent TSEN cleavage sites mutated to C (*CBP1-3AC*). In *xrn1Δ*, the 3′ cleavage products are detectable for CBP1, but are reduced for the *CBP1-3AC* mutant. This panel shows a representative blot. (*C* and *D*) The level of the cleaved mRNA relative to full-length mRNA was quantitated and normalized in *xrn1Δ* (*C*) and *ski7Δ* (*D*) mutants. The values for individual biological replicates are plotted (circles) as is the average (horizontal bar) and SD (error bar). The 3′ cleavage product that accumulates in *xrn1Δ* is quantitated in *C* and the 5′ cleavage product that accumulates in *ski7Δ* is quantitated in *D*. (*E*) Wild-type *CBP1* is efficiently cleaved by recombinant TSEN in vitro, but this cleavage is strongly reduced for the *CBP1-3AC* mutant. The numbers below the gel indicate percent substrate cleaved in this experiment, which is representative of triplicates. Note that the 46-nt substrate contains fewer labeled nucleotides than the 170- and 75-nt substrates, which explains why the product bands appear lighter than the same amount of substrate. Numbers to the left are sizes of the pre-tRNA–Phe [specifically, tF(GAA)F] substrate and products (18-nt intron, 38- and 39-nt exons, 56 and 57 singly cut RNAs consisting of intron and one exon). Numbers and schematic to the right is a summary of product size expected for the 75-nt substrate based on the in vivo cleavage sites (*SI Appendix*, Table S3). Predicted products depicted as black lines are prominent in the gel, while products depicted in gray are not. Shown is a representative gel. A replicate with an independently purified second batch of enzyme and RNA is shown in *SI Appendix*, Fig. S2.

50 and 7 nt). This is in good agreement with the major band produced from wild-type *CBP1* substrate migrating slightly slower that the pre-tRNA–Phe exons of 38 and 39 nt, a second band comigrating with the 18-nt pre-tRNA intron, and a third even smaller band. When we used a substrate with extended 5′ and 3′ ends it also produced the 46-nt product, confirming that this is an internal fragment, but it produced longer terminal fragments as expected (~60 nt instead of 18 and 11). Importantly, production of the 46-nt product was reduced more than 10-fold for the *CBP1-3AC* RNA, and instead a product of ~57 nt was prominent. This 57-nt product is consistent with cleavage only at 669, and shows striking similarity to in vitro products of the enzyme with a *sen2-H297A* mutation (25) (*Discussion*). In addition to the change in major product from 46 to 57 nt, the *CBP1-3AC* mutant was cleaved approximately twofold less (13% vs. 6%, when considering the 46- and 57-nt products cumulatively, and correcting for the number of labeled U residues). This overall reduction in cleavage is in good agreement with the two- to threefold reduction seen in vivo. Thus, the in vitro results indicate that cleavage at nucleotide 715 is strongly reduced in the *CBP1-3AC* mutant.

The Sen2 Catalytic Histidine Is Required for Cleavage at All Sites In Vivo. TSEN contains two catalytic sites with catalytic histidine residues in Sen2 (His297) and Sen34 (His217). In vitro, *sen2-H297A* prevents cleavage between the 5′ exon and intron (5′ site) of pre-tRNA, while *sen34-H217A* prevents cleavage of the 3′ site (23). In contrast, in vivo *sen2-H297A* causes accumulation of pre-tRNAs that are end-matured but contain both exons and the intron (26), suggesting that *sen2-H297A* prevents cleavage at both the 5′ and 3′ sites in vivo. To investigate the role of Sen2-H297 more broadly, we repeated PARE analysis. For this analysis we used the *sen2-ts xrn1Δ* strain used above, and transformed it with either a wild-type *SEN2* plasmid, a *sen2-H297A* plasmid, or an empty vector. RNA was extracted from duplicate cultures, and all six RNA samples were analyzed by PARE. We then calculated the comPARE scores for all known TSEN sites, including the 5′ and 3′ sites of all pre-tRNA introns and the sites in the *CBP1*, *MIS1*, *ERV1*, *COQ5*, and *PKP2* mRNAs. In these comPARE analyses, we compared the strain containing the wild-type *SEN2* plasmid to either the strain with the *sen2-H297A* plasmid or the empty vector strain. In Fig. 6*A* the comPARE scores of known TSEN sites for replicate 1 of *sen2-H297A* are plotted against the comPARE scores for empty vector, revealing a strong correlation with a slope near 1. This indicates that in vivo the *sen2-H297A* complementing plasmid is defective in cleaving both 5′ sites and 3′ sites in pre-tRNA as well as mRNA sites. Fig. 6*B* shows the correlation coefficients for each of the replicates of *sen2-H297A* and

empty vector, indicating that the comPARE scores for *sen2-H297A* and empty vector are as strongly correlated with each other as with their biological replicate. Thus, we conclude that Sen2-H297 is required for all TSEN-mediated cleavages in vivo, possibly because it has a role in substrate binding in addition to its catalytic role (*Discussion*).

TSEN Cleaves the Same mRNAs during Fermentative and Respiratory Growth. Yeast has two main metabolic growth states that differ greatly by their mitochondrial activity. In the presence of glucose, yeast ferments glucose to ethanol, with mitochondrial respiration being largely inactive. Genes such as *CBP1* and *COQ5* are non-essential under these conditions (yeastgenome.org). The above PARE analysis was performed in either YEP (Figs. 1 and 3) or SC-Leu media (Fig. 6), both containing glucose. Alternatively, when provided with carbon sources that cannot be fermented (such as glycerol), yeast will grow by respiration, mitochondria are more numerous and more active, and *CBP1* and *COQ5* are essential (yeastgenome.org). Because TSEN is localized to the outside of mitochondria and appears to target mRNAs that encode mitochondrial proteins, we repeated PARE analysis of the *xrn1Δ* and *xrn1Δ sen2-ts* strains grown in YEP+2% glycerol. This analysis revealed that TSEN targeted mRNAs are cleaved in both growth conditions (Fig. 7 and *SI Appendix*, Figs. S1 and S3).

We next generated a list of genes that scored high in a majority of the seven comPARE datasets by filtering sites that had a PARE score >1 in the *xrn1Δ* sample and a comPARE score >3 when compared to the matching *xrn1Δ sen2* sample in at least four of the seven comPARE datasets (Fig. 7*A* and *SI Appendix*, Table S1). This list contains five pre-tRNA splice sites in four different pre-tRNAs (Fig. 7*A*). Two of these are 5′ sites and three are 3′ sites. Also included in the recurrent sites were 33 sites in 22 different ORFS, as well as 1 site in the intergenic region between *PAN6* and *ATG32*. Ten of these sites had a comPARE score >3 in all seven datasets, and a good match to the sequence motif in Fig. 5*A* and thus the corresponding mRNAs are high-confidence TED targets (*CBP1*, *COQ5*, *PKP2*, *DLD1*, and *ERV1*) (*SI Appendix*, Table S1). These five mRNAs each encode mitochondrial proteins (51–53). Three other mRNAs have comPARE scores >3 in six of the seven datasets and match well to the sequence motif (*MIS1*, *YHR033W*, *MDL1*). *MIS1* appears to be not expressed in the seventh dataset, while *YHR033W* and *MDL1* have comPARE scores of 2.96 and 2.87 in one of the datasets, just barely below the applied cutoff of 3. The Mis1, Mdl1, and YHR033W proteins are also mitochondrial (51–53). Thus, we conclude that these eight mRNAs are very likely TED targets. Some of the other mRNAs in Fig. 7*A* may also be TED targets, but some of them may be false positives (e.g., YBL059W) even though they had comPARE scores >3 in at least half of the datasets.

Gene ontology (GO) analysis (https://yeastgenome.org/goTermFinder) of the 22 ORFs from Fig. 7*A* for enrichment in cellular components revealed an enrichment for mitochondrial proteins. Thirteen of the 22 ORFs are annotated with the GO term "mitochondria" ($P = 0.0011$) (Fig. 7*A*). Nine of these are annotated with "mitochondrial envelope" ($P = 0.00028$). Several similar GO categories were also enriched (e.g., mitochondrial part, mitochondrial membrane, organelle envelope). However, there are 1,237 genes annotated with "mitochondria" and 457 with "mitochondrial envelope," indicating that TED targets only a small subset of them. Similar GO analysis for enrichment in functional categories revealed an enrichment for "nucleotide binding" (10 proteins, $P = 0.0086$), while no particular process category was enriched. Of the 10 "nucleotide binding" proteins, 7 were mitochondrial. Overall, qualitative comparison of these seven comPARE datasets suggests that the same mRNAs that code for mitochondrial proteins are reproducibly cleaved by TSEN under various conditions.

Finally, we used PARE signals to compare the contributions of TED and decapping to mRNA decay. Both TED and decapping products accumulate as 5′ phosphorylated products in the *xrn1Δ* strain. Thus, we used the PARE peaks upstream of ORFs as a measure of decapping and compared the TSEN-dependent PARE peaks to these putative decapping PARE peaks for the eight highest-confidence TED targets. Fig. 7*B* shows the fraction of TSEN products relative to the total degradome (TSEN cleavage plus decapping) for these genes. This revealed two trends. First, as we expected the contribution of TED to mRNA degradation varied between mRNAs. When the signals for the four glucose grown samples were averaged (horizontal bars in Fig. 7*B*), for *CBP1*, *ERV1*, and *PKP2* the PARE signal from TED was similar to the decapping PARE signal, suggesting that both pathways contribute approximately equally to their degradation. For the five other high-confidence TED targets, TSEN products were

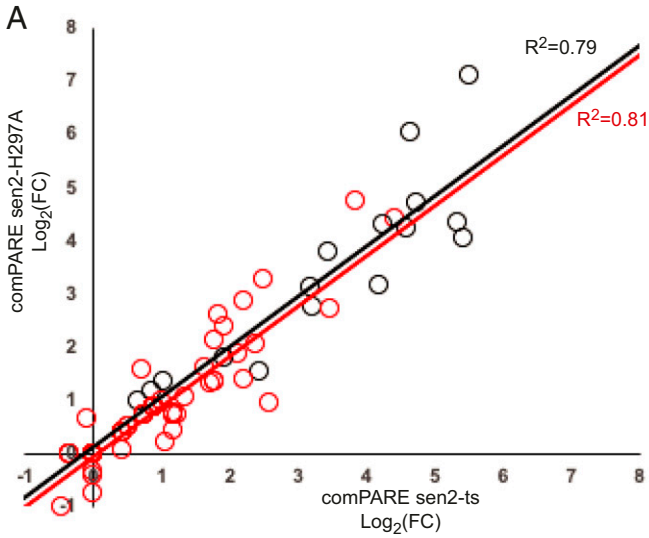

Fig. 6. All TSEN-dependent cleavages detected by comPARE require Sen2-H297. (*A*) Plotted are the comPARE scores for one biological replicate of *xrn1Δ sen2-ts* with an empty vector plotted against the comPARE score of the same strain with a *sen2-H297A* plasmid. Data from pre-tRNA splice sites are in red, while data from mRNA sites from Fig. 3 are in black. Cleavage sites requiring Sen2-H297 fall along a line with slope 1, while Sen2-H297–independent (and presumably Sen34-H217–dependent) sites should fall along the *x* axis. The data points cluster along the diagonal and are correlated with an $R^2 = 0.79$ for all the mRNA sites and $R^2 = 0.81$ for all the pre-tRNA splice sites. (*B*) Correlation coefficients of two biological replicates of empty vector and two biological replicates of *sen2-H297A* indicate that essentially all in vivo-detected TSEN-dependent cleavages require the His297 residue of Sen2. The correlation coefficients include both the pre-tRNA and mRNA sites.

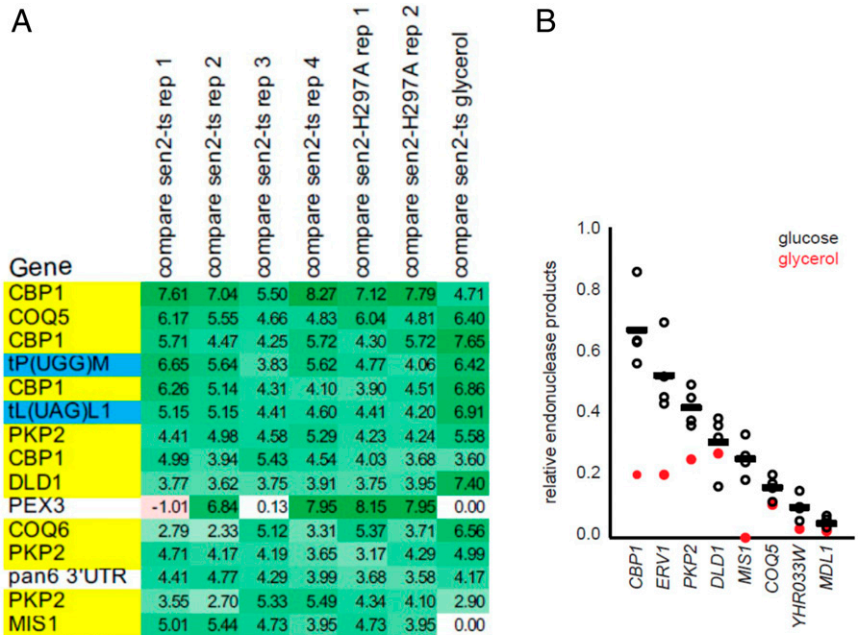

Gene	compare sen2-ts rep 1	compare sen2-ts rep 2	compare sen2-ts rep 3	compare sen2-ts rep 4	compare sen2-H297A rep 1	compare sen2-H297A rep 2	compare sen2-ts glycerol
CBP1	7.61	7.04	5.50	8.27	7.12	7.79	4.71
COQ5	6.17	5.55	4.66	4.83	6.04	4.81	6.40
CBP1	5.71	4.47	4.25	5.72	4.30	5.72	7.65
tP(UGG)M	6.65	5.64	3.83	5.62	4.77	4.06	6.42
CBP1	6.26	5.14	4.31	4.10	3.90	4.51	6.86
tL(UAG)L1	5.15	5.15	4.41	4.60	4.41	4.20	6.91
PKP2	4.41	4.98	4.58	5.29	4.23	4.24	5.58
CBP1	4.99	3.94	5.43	4.54	4.03	3.68	3.60
DLD1	3.77	3.62	3.75	3.91	3.75	3.95	7.40
PEX3	-1.01	6.84	0.13	7.95	8.15	7.95	0.00
COQ6	2.79	2.33	5.12	3.31	5.37	3.71	6.56
PKP2	4.71	4.17	4.19	3.65	3.17	4.29	4.99
pan6 3'UTR	4.41	4.77	4.29	3.99	3.68	3.58	4.17
PKP2	3.55	2.70	5.33	5.49	4.34	4.10	2.90
MIS1	5.01	5.44	4.73	3.95	4.73	3.95	0.00
YHR033W	4.55	3.73	2.96	3.86	3.05	4.37	5.15
MDL1	3.44	4.22	3.91	3.35	4.37	2.87	5.00
tP(UGG)O1	2.84	3.71	3.47	4.60	2.72	4.12	5.35
BUD32	3.96	2.73	3.80	3.80	3.44	4.09	4.57
SWT1	3.13	3.58	2.92	4.68	3.18	3.96	4.95
COQ6	1.13	3.29	5.84	2.96	5.23	3.83	2.84
KTR3	3.66	2.70	3.10	3.01	3.19	3.05	6.41
ERV1	4.39	3.68	3.19	3.07	3.13	3.47	4.05
YIR016W	1.55	1.58	3.01	3.87	3.05	3.39	8.30
TAH11	3.53	2.77	3.40	2.85	2.88	3.38	5.35
VMS1	2.57	2.67	3.20	4.79	2.60	3.43	4.79
TUF1	2.75	3.36	2.81	3.83	3.48	3.36	3.93
tP(UGG)O1	3.20	3.50	2.13	4.65	1.86	4.65	3.30
PHB2	1.38	3.12	3.52	4.01	3.21	2.44	5.23
COQ5	3.75	2.68	3.43	2.58	3.79	2.04	4.23
TUF1	3.24	2.14	2.55	3.82	3.35	3.35	3.96
ABP1	4.00	2.88	3.05	4.30	3.99	2.70	1.39
PKP2	3.10	2.30	3.21	4.15	2.74	4.02	2.22
NAT1	4.47	2.80	3.01	2.11	3.21	1.21	4.68
MIS1	3.43	3.75	3.16	2.92	3.16	2.44	0.54
tY(GUA)F1	2.42	3.24	2.49	3.82	3.29	3.82	0.00
PEX3	-0.28	4.77	-0.11	4.48	4.62	4.08	0.00
YBL059W	-1.40	7.62	-7.02	7.27	-6.86	8.92	3.30
RPS14A	-4.62	-0.48	3.08	3.18	3.16	3.63	1.45

Fig. 7. Summary of seven comPARE datasets from different conditions. (*A*) Shown are 39 sites that in the majority (at least 4 of 7) of the datasets had a PARE score >1 and a comPARE score >3. comPARE scores are shown and shaded from high (dark green) to low (dark red). The 39 sites are listed in order of average comPARE score. Yellow highlighted genes encode mitochondrial proteins, while cyan highlighted genes encode intron containing pre-tRNAs. A more extensive version is included as *SI Appendix*, Table S1. (*B*) Endonuclease cleavage contributes substantially to mRNA decay. To estimate the contribution of TSEN to mRNA degradation the major PARE signals attributable to endonucleolytic cleavage were compared to the total degradome signal (PARE peaks attributable to TSEN plus PARE peaks attributable to decapping). Thus, a value of 1 would reflect exclusive degradation by TSEN, while a value of 0.5 reflects equal contributions of TSEN and decapping to mRNA decay.

less abundant than decapping products under these conditions, contributing less than 30% of the total mRNA degradome. However, even for these genes the TSEN product made a substantial contribution to the overall degradome. Second, in the glycerol sample, the prominence of TED was reduced relative to decapping for all eight high-confidence TED targets when compared to the average of the glucose samples (Fig. 7*B*, compare the red dots to the bars). Determining whether this reduced contribution of TED reflects the difference between respiratory and fermentative growth will require additional studies, but it does suggest that the quantitative contribution of TED to mRNA decay varies between conditions. Overall, this comparison between TED and decapping activities suggests that the contribution of TED to mRNA decay is considerable but varies both between mRNAs and conditions (*Discussion*).

Discussion

PARE and comPARE Identify Endonuclease Cleavages Sites. PARE was developed to identify endonuclease cleavage sites and has been used to identify the mRNA degradome that accumulates upon deletion or depletion of *XRN1*. Here we use this strategy to characterize the function of two endoribonucleases, the RNA exosome and TSEN, by identifying PARE scores reduced in the corresponding mutant. Because the RNA exosome is both nuclear and cytoplasmic, we used an *xrn1Δ rat1-1* double mutant. Notably this characterization of the nuclear degradome available

to the community is unique, but we still were unable to identify any convincing endonuclease cleavage sites for the PIN domain of the RNA exosome. In contrast, we identified novel and known TSEN cleavage sites. One possible explanation is that the RNA exosome may have a lower specificity for specific positions than the TSEN complex, which exhibits strong preference to cleave specific sites. In addition, PARE is designed to detect polyadenylated products, and the PIN domain of the RNA exosome may cleave unadenylated substrates. We further developed a simple bioinformatic pipeline (comPARE) that identifies cleavage sites with single nucleotide precision. comPARE should be readily implementable by RNA biologists studying a variety of processes. Through the powerful method of PARE and comPARE, we provide an expanded understanding of TSEN function.

The Expanding Function of TSEN. TSEN was initially discovered as an endonuclease with a dedicated function in tRNA splicing (49, 59), and was studied for many years for this role (Fig. 8*A*). Here we show that TSEN cleaves multiple mRNAs that encode mitochondrial proteins and propose to name this pathway TED (Fig. 8*B*). One puzzling aspect of yeast TSEN was that it localized to the outside of mitochondria, which provides no obvious advantage for a nuclease dedicated to pre-tRNA splicing. Furthermore, although TSEN is assembled more efficiently in its native location, it is able to assemble and effectively splice tRNAs when artificially localized into the nucleus (26, 60). The role of TSEN in cleaving mRNAs that encode mitochondrial proteins provides a rational explanation for its localization.

We note that archaeal TSEN also cleaves at least one mRNA (61), suggesting that TED may be an ancient conserved pathway. The targets of TED are likely to differ in different organisms. For example, archaeal TSEN targets the cbf5 mRNA (61), which we did not detect as a yeast target. Unlike yeast TSEN, human TSEN is a nuclear enzyme (62), and thus it appears unlikely that human TED targets mRNAs that encode mitochondrial proteins. Instead, if human TSEN cleaves mRNAs, the target mRNAs are likely to differ from the ones in yeast.

While TSEN produces 5′ hydroxyl RNAs, Xrn1 only degrades 5′ monophosphate RNAs, and PARE only detects RNAs that have a 5′ monophosphate. This implies that there must be some kinase that phosphorylates TED targets. Based on its known function in other kinase-dependent mRNA decay pathways, Trl1 appears the most likely candidate (63, 64), but its role will require further investigation (Fig. 8*B*). Interestingly, human TSEN associates with the polynucleotide kinase CLP1 (62, 65, 66). While the human pre-tRNA splicing mechanism does not require a polynucleotide kinase step, if human TSEN also cleaves other RNAs to initiate their degradation by XRN1 or XRN2, this would require a polynucleotide kinase such as CLP1.

Remarkably, mutations in either human TSEN or CLP1 cause pontocerebellar hypoplasia (67–69). Based on several observations we speculate that a defect in TED may be more relevant to this disease than tRNA splicing. First, human tRNA splicing also requires the ligase RTCB (Fig. 8*A*), but mutations in *RTCB* have not been found in pontocerebellar hypoplasia patients. Second, as mentioned, TED requires both TSEN and a polynucleotide kinase such as CLP1, but the distinct human tRNA splicing pathway does not require phosphorylation of an intermediate RNA (Fig. 8*A*). Third, fibroblasts and induced neurons of pontocerebellar patients with *CLP1* mutations accumulated higher levels of some intron-containing pre-tRNAs compared to unaffected controls, but other intron-containing pre-tRNAs were less abundant in patient cells (68). Thus, pre-tRNA levels were not consistently affected in CLP1 pontocerebellar patient cells, consistent with the absence of an RNA phosphorylation step in the human pre-tRNA splicing pathway. Whether a defect in TED indeed underlies pontocerebellar hypoplasia will be difficult to test, but a strategy similar to ours should be able to identify the substrates for such a pathway.

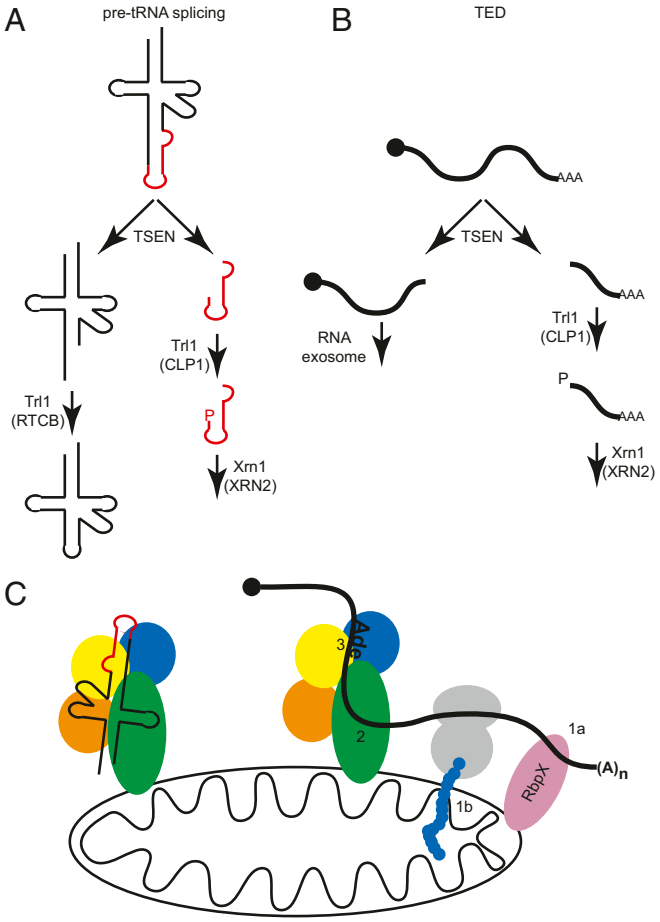

Fig. 8. An expanded view of TSEN function. (*A*) The pre-tRNA splicing pathway is depicted. TSEN cleaves the pre-tRNA. In yeast, the resulting exons (black lines) are ligated by Trl1 in multiple steps, while in humans this is carried out in a single step by RTCB. The released yeast introns (red lines) are degraded by Xrn1 after phosphorylation by Trl1. In humans this presumably is carried out by CLP1 and XRN2. (*B*) The TED pathway is depicted, which includes cleavage by TSEN, degradation of the 5′ product by the RNA exosome, and degradation of the 3′ product by Xrn1 (XRN2 in humans) after phosphorylation by Trl1 [CLP1 in humans (80)]. (*C*) Shown on the left is the previously proposed ruler model, where Sen54 recognizes tRNA structure at sites distant from the actual cleavage sites. Sen54 has also been proposed to be required for targeting to the mitochondrial outer membrane. The evidence that both of these roles are carried out by Sen54 is incomplete and other subunits may also contribute. Shown on the right is that mRNAs are known to be localized to the mitochondrial membrane either by RNA binding proteins (RbpX) binding to their 3′ UTR (marked 1a), or through cotranslational import of the nascent protein (marked 1b). We propose that this colocalization is required but not sufficient for TSEN-mediated cleavage. The cleavage sites are proposed to be determined by additional interactions between TSEN (perhaps Sen54) and mRNA features distal from the cleavage sites (marked 2) and interaction between the active sites of Sen2 and Sen15 and mRNA features proximal to the cleavage sites (marked 3), including an A at −1 (indicated as Ade).

We suspect that our high-confidence list of TED targets might be incomplete. As discussed, the standard implementation of PARE focused on poly(A)+ RNAs that have a 5′ monophosphate, and library preparation includes a size-selection step. Thus, TSEN could produce some cleavage products that either lack a poly(A) tail, are not 5′ phosphorylated after cleavage, or are too small for this RNA isolation and sequencing strategy. We also suspect that the stringent cut-offs we used limit the detection of some sites. For example, we note that in addition to the high-confidence site

in *ERV1* there is a lower scoring site 35 nt upstream (*SI Appendix*, Fig. S3) that is detectable in the *SEN2* strain, but reduced in the *sen2-ts* strain, with an average comPARE score of 2.4. Strikingly, cleavage at this site could explain the in vitro cleavage product of about 35 and 26 nt in Fig. 4. We thus speculate that this is an authentic TSEN site in vivo and in vitro and other similar sites remain to be determined.

We suspect that the cleavage of the mRNAs we identified is not the unknown essential function of TSEN. TSEN inactivation would result in overexpression of TED targets, but none of the TED targets are known to be lethal when individually overexpressed (70). We therefore conclude that cleavage/degradation of the mRNAs we identified is an unlikely explanation for the lethality of TSEN inactivation. *ERV1* is the only essential gene we identified as a TED target, but its sole intron is a typical spliceosomal intron and TSEN does not appear to have a function in splicing *ERV1* pre-mRNA. Thus, TSEN is unlikely to be required for Erv1 expression. While it is known that TSEN mutations (likely indirectly) affect ribosomal RNA processing (26), none of the targets we discovered seem to be involved in preribosomal RNA processing. Overall, we conclude that although we have expanded our understanding of TSEN function, our knowledge remains incomplete and the unknown essential function of TSEN remains to be determined.

A Model for TED. In the absence of structural information, substrate recognition by eukaryotic TSEN remains poorly understood. Biochemical studies have revealed multifaceted recognition of pre-tRNAs that combines proximal and distal recognition sites. Specifically, pre-tRNA cleavage requires a base pair between the anticodon loop and intron (the A-I base pair) (56, 58, 71, 72), but is also determined by the distance between the cleavage site and the body of the tRNA (55, 57). This has led to the proposal of a ruler model, where the overall structure of tRNA is recognized by TSEN, perhaps by the Sen54 subunit, and cleavage occurs at a specific distance from this recognition site (Fig. 8*C*, left side). Archaeal and eukaryotic TSEN also recognize a short helix within its targets (72, 73). TSEN was also hypothesized to recognize a stem loop structure in *CBP1* (25) but the stem loop was solely proposed based on mFOLD prediction, and its importance was not tested through compensatory mutations. In our hands mFOLD, RNAfold, and TurboFold did not suggest convincing structures for any of the TED substrates. We therefore suggest that future in vivo and in vitro experiments are needed to fully understand the structures of pre-tRNA and mRNA that are recognized by TSEN.

For TED, we propose a model that explains most of our and previously published data (Fig. 8*C*, right side) and shares aspects with the ruler model for pre-tRNA cleavage. In this modified ruler model, recognition of substrate mRNAs occurs in at least three steps. First, TED requires that target mRNAs are localized with TSEN on the outside of mitochondria (step 1 in Fig. 8*C*). mRNAs can be localized to mitochondria through interactions with RNA binding proteins that bind simultaneously to their target mRNAs and mitochondria (step 1a in Fig. 8*C*) or through the cotranslational recognition of the nascent peptide by the TOM protein import machinery (step 1b in Fig. 8*C*) (74–76). Similarly, translation of the CBP1 transit peptide has been shown to be required for TED (25). This colocalization contributes to which mRNAs are cleaved, but not what sites are cleaved. Second, we suspect that mRNAs are recognized by a distal substrate recognition site and cleaved some distance away. This would explain why several TED targets are cleaved at a small number of clustered sites: Recognizing one distal site may allow cleavage at a cluster of sites. Furthermore, this explains why overexpressed *CBP1* is cleaved at sites that are not efficiently cleaved in the endogenous mRNA. Such distal recognition also explains why a 170-nt *CBP1* fragment was cleaved more efficiently than a shorter substrate in vitro (Fig. 5*E*). Whether distal recognition of mRNAs requires the same binding site on TSEN as for the tRNA ruler mechanism remains to be determined. Finally, interactions between the substrate and enzyme near the catalytic center position the phosphodiester backbone precisely in the active site (step 3 in Fig. 8*C*). This appears to involve an interaction between the −1A base and the enzyme. Remarkably, mutating the −1A bases in *CBP1* (Fig. 5*D*) has a very similar effect to mutating Sen2-His297 in vitro (25). A possible explanation is that the −1A nucleotide is recognized in proximity to the Sen2 catalytic histidine. In archaea, the equivalent His is stacked onto base +1 of the substrate RNA (77). We therefore suggest that Sen2-H297 and the −1A both contribute to substrate recognition, but do not directly interact with each other. A role of Sen2-H297 in substrate binding also explains our observation and previous observations (26) that the *sen2-H297A* mutation prevents cleavage at all TSEN sites in vivo.

Although the overall ruler model for pre-tRNA recognition can be extended to TED, the details of substrate recognition are likely to differ. Specifically, we find a preference for A at −1 for mRNA cleavage, that has not been described for pre-tRNA splice sites. Instead, the 5′ pre-tRNA splice sites appear to have very little if any sequence specificity (*SI Appendix*, Fig. S4). Extensive biochemical and structural approaches will be needed to fill in these details of substrate recognition.

Implications for Regulation of TED. Because TSEN has a critical role in tRNA production, regulation of TED by changing the activity of TSEN is unlikely under most conditions. However, slower growth requires lower rates of tRNA synthesis and splicing. A possibly lower amount of TSEN, combined with increased expression of mitochondrial proteins, may be related to our initial analysis that suggests that TED might be less active during slower respiratory growth on glycerol, but more research will be needed to establish how this occurs.

Our proposed multistep substrate recognition model (Fig. 8*C*, right side) has several additional implications for TED regulation. First, although mRNAs that encode mitochondrial proteins are enriched on the outside of the mitochondria, these mRNAs are also present diffusely in the cytoplasm. For any given gene, TED can only cleave the subset of mRNA molecules that are localized near the mitochondria, while decapping is likely to degrade the more diffuse mRNA molecules from the same gene. It seems likely that cotranslational import of proteins into the mitochondria is more efficient than posttranslational import of diffusely produced protein. Thus, while TED and decapping may overall contribute similarly to the degradation of TED mRNA targets—such as *CBP1*, *ERV1*, and *PKP2* (Fig. 7*B*)—by targeting the localized mRNA, TED might have a disproportionate impact on protein levels by degrading mRNAs actively involved in cotranslational import.

A second implication of our model is that any physiological condition that affects the localization of TED targets also is likely to alter the balance between TED and decapping. Similarly, alterations in TED target structure or in protein binding near TSEN recognition sites are likely to alter the balance between TED and decapping. This may explain condition-specific differences in TSEN-mediated and decapping-mediated decay (Fig. 7*B*).

A third implication of our model is that in vitro cleavage assays only reflect steps 2 and 3 of the model and do not reflect the contribution of colocalization to substrate specificity. This colocalization and the multiple interactions between TSEN, mitochondria, and TED targets is likely to increase the avidity of TSEN for TED targets in vivo. In contrast to TED targets, pre-tRNAs are not known to be actively targeted to the mitochondria. Thus, one reason why mRNA substrates are a poorer substrate in vitro when compared to pre-tRNA may be that the in vitro system is missing an important aspect of in vivo mRNA avidity but the

same in vitro conditions may fully reflect the affinity for pre-tRNAs.

Similarities between TED and RIDD. Several aspects of TED are similar to the ER-localized RIDD pathway. First, mRNA degradation is initiated by an endonuclease that is bound to a specific membrane (the ER membrane and the mitochondrial outer membrane). Second, mRNAs are targeted in part due to their colocalization with the enzyme, and this mRNA localization depends partially on the cotranslational import of the encoded nascent protein into the organelle. Third, the endonuclease shows some, but limited sequence specificity (UGC at −2 to +1 for RIDD) (18). Fourth, the resulting fragments are degraded by the RNA exosome and Xrn1 (18, 21). Fifth, the endoribonuclease cleavage produces a 5′ hydroxyl, which is converted to a 5′ monophosphate that allows degradation by Xrn1 in vivo and that is exploited by PARE. Given the similarities between the two pathways, we speculate that other mRNA decay pathways initiated by localized endonucleases remain to be discovered. Possible locations for these pathways include the chloroplast outer membrane and highly polarized cell projections such as those found in neurons of Metazoa and hyphae of Fungi.

Materials and Methods

All yeast strains and plasmids were created by standard methods. Yeast was grown to mid-log phase at room temperature, incubated at 37 °C for 1 h to inactivate *sen2-ts* or *rat1-1*, and RNA was extracted as previously described (78). PARE analysis for Fig. 1 was performed as previously described (79), or performed by LCSciences by a slightly different protocol. RNA sequencing reads have been deposited in the Sequence Read Archive (SRA) under accession no. PRJNA663967. All data analysis was performed on a Galaxy server using "FastQC,", "TopHat," "bamCoverage," and "bigwigCompare." RNA structures were predicted using mFOLD, RNAfold, and TurboFold. Sequence logos were generated at https://weblogo.berkeley.edu/logo.cgi. GO analysis was performed at https://yeastgenome.org/. Recombinant TSEN was purified from a baculovirus system. Endonuclease assays were performed at least three times on each of the mRNA substrates, using duplicate preparations of independently expressed and purified protein. Additional details on methods can be found in *SI Appendix*.

Data Availibility. RNA-sequencing data have been deposited in the National Center for Biotechnology Information SRA, https://www.ncbi.nlm.nih.gov/sra (accession no. PRJNA663967) (81).

ACKNOWLEDGMENTS. We thank Pamela J. Green for her support; the A.v.H. laboratory for thoughtful discussions; Jay Hesselberth, Scott Gradia, and Addgene for plasmids; and Phil Hieter for the *sen2-ts* strain. This work was funded by NIH Grant R01GM130147 (to A.v.H. and Anita Corbett) and the Cancer Prevention Research Institute of Texas Grant 13127 (to CPRIT Scholar in Cancer Research, K.-L.T.). Vinay K. Nagarajan was supported by NSF Grant MCB1817764 (to Pamela J. Green). M.A.S. was in part supported by departmental Welch Foundation Grant AV-0024.

1. A. W. Johnson, Rat1p and Xrn1p are functionally interchangeable exoribonucleases that are restricted to and required in the nucleus and cytoplasm, respectively. *Mol. Cell. Biol.* **17**, 6122–6130 (1997).
2. A. Stevens, T. L. Poole, 5′-exonuclease-2 of Saccharomyces cerevisiae. Purification and features of ribonuclease activity with comparison to 5′-exonuclease-1. *J. Biol. Chem.* **270**, 16063–16069 (1995).
3. A. Chlebowski, M. Lubas, T. H. Jensen, A. Dziembowski, RNA decay machines: The exosome. *Biochim. Biophys. Acta BBA* **1829**, 552–560 (2013).
4. E. V. Wasmuth, C. D. Lima, Structure and activities of the eukaryotic RNA exosome. *Enzymes* **31**, 53–75 (2012).
5. A. van Hoof, P. A. Frischmeyer, H. C. Dietz, R. Parker, Exosome-mediated recognition and degradation of mRNAs lacking a termination codon. *Science* **295**, 2262–2264 (2002).
6. K. Januszyk, C. D. Lima, The eukaryotic RNA exosome. *Curr. Opin. Struct. Biol.* **24**, 132–140 (2014).
7. V. K. Nagarajan, C. I. Jones, S. F. Newbury, P. J. Green, XRN 5′→3′ exoribonucleases: Structure, mechanisms and functions. *Biochim. Biophys. Acta* **1829**, 590–603 (2013).
8. A. J. Pratt, I. J. MacRae, The RNA-induced silencing complex: A versatile gene-silencing machine. *J. Biol. Chem.* **284**, 17897–17901 (2009).
9. W. F. Lima, C. L. De Hoyos, X. H. Liang, S. T. Crooke, RNA cleavage products generated by antisense oligonucleotides and siRNAs are processed by the RNA surveillance machinery. *Nucleic Acids Res.* **44**, 3351–3363 (2016).
10. T. I. Orban, E. Izaurralde, Decay of mRNAs targeted by RISC requires XRN1, the Ski complex, and the exosome. *RNA* **11**, 459–469 (2005).
11. M. A. Getz, D. E. Weinberg, I. A. Drinnenberg, G. R. Fink, D. P. Bartel, Xrn1p acts at multiple steps in the budding-yeast RNAi pathway to enhance the efficiency of silencing. *Nucleic Acids Res.* **48**, 7404–7420 (2020).
12. F. F. Souret, J. P. Kastenmayer, P. J. Green, AtXRN4 degrades mRNA in Arabidopsis and its substrates include selected miRNA targets. *Mol. Cell* **15**, 173–183 (2004).
13. A. B. Eberle, S. Lykke-Andersen, O. Mühlemann, T. H. Jensen, SMG6 promotes endonucleolytic cleavage of nonsense mRNA in human cells. *Nat. Struct. Mol. Biol.* **16**, 49–55 (2009).
14. E. Huntzinger, I. Kashima, M. Fauser, J. Saulière, E. Izaurralde, SMG6 is the catalytic endonuclease that cleaves mRNAs containing nonsense codons in metazoan. *RNA* **14**, 2609–2617 (2008).
15. C. Sidrauski, P. Walter, The transmembrane kinase Ire1p is a site-specific endonuclease that initiates mRNA splicing in the unfolded protein response. *Cell* **90**, 1031–1039 (1997).
16. T. N. Gonzalez, C. Sidrauski, S. Dörfler, P. Walter, Mechanism of non-spliceosomal mRNA splicing in the unfolded protein response pathway. *EMBO J.* **18**, 3119–3132 (1999).
17. D. Ron, P. Walter, Signal integration in the endoplasmic reticulum unfolded protein response. *Nat. Rev. Mol. Cell Biol.* **8**, 519–529 (2007).
18. P. Kimmig *et al.*, The unfolded protein response in fission yeast modulates stability of select mRNAs to maintain protein homeostasis. *eLife* **1**, e00048 (2012).
19. J. Hollien *et al.*, Regulated Ire1-dependent decay of messenger RNAs in mammalian cells. *J. Cell Biol.* **186**, 323–331 (2009).
20. K. Mishiba *et al.*, Defects in IRE1 enhance cell death and fail to degrade mRNAs encoding secretory pathway proteins in the Arabidopsis unfolded protein response. *Proc. Natl. Acad. Sci. U.S.A.* **110**, 5713–5718 (2013).
21. J. Hollien, J. S. Weissman, Decay of endoplasmic reticulum-localized mRNAs during the unfolded protein response. *Science* **313**, 104–107 (2006).
22. J. Abelson, C. R. Trotta, H. Li, tRNA splicing. *J. Biol. Chem.* **273**, 12685–12688 (1998).
23. C. R. Trotta, S. V. Paushkin, M. Patel, H. Li, S. W. Peltz, Cleavage of pre-tRNAs by the splicing endonuclease requires a composite active site. *Nature* **441**, 375–377 (2006).
24. R. Rauhut, P. R. Green, J. Abelson, Yeast tRNA-splicing endonuclease is a heterotrimeric enzyme. *J. Biol. Chem.* **265**, 18180–18184 (1990).
25. T. Tsuboi *et al.*, The tRNA splicing endonuclease complex cleaves the mitochondria-localized CBP1 mRNA. *J. Biol. Chem.* **290**, 16021–16030 (2015).
26. N. Dhungel, A. K. Hopper, Beyond tRNA cleavage: Novel essential function for yeast tRNA splicing endonuclease unrelated to tRNA processing. *Genes Dev.* **26**, 503–514 (2012).
27. P. D. Cherry, L. K. White, K. York, J. R. Hesselberth, Genetic bypass of essential RNA repair enzymes in budding yeast. *RNA* **24**, 313–323 (2018).
28. C. E. Shamu, P. Walter, Oligomerization and phosphorylation of the Ire1p kinase during intracellular signaling from the endoplasmic reticulum to the nucleus. *EMBO J.* **15**, 3028–3039 (1996).
29. J. S. Cox, C. E. Shamu, P. Walter, Transcriptional induction of genes encoding endoplasmic reticulum resident proteins requires a transmembrane protein kinase. *Cell* **73**, 1197–1206 (1993).
30. K. Mori, W. Ma, M. J. Gething, J. Sambrook, A transmembrane protein with a cdc2+/CDC28-related kinase activity is required for signaling from the ER to the nucleus. *Cell* **74**, 743–756 (1993).
31. T. Yoshihisa, K. Yunoki-Esaki, C. Ohshima, N. Tanaka, T. Endo, Possibility of cytoplasmic pre-tRNA splicing: The yeast tRNA splicing endonuclease mainly localizes on the mitochondria. *Mol. Biol. Cell* **14**, 3266–3279 (2003).
32. T. Yoshihisa, C. Ohshima, K. Yunoki-Esaki, T. Endo, Cytoplasmic splicing of tRNA in Saccharomyces cerevisiae. *Genes Cells* **12**, 285–297 (2007).
33. K. Moore, J. Hollien, Ire1-mediated decay in mammalian cells relies on mRNA sequence, structure, and translational status. *Mol. Biol. Cell* **26**, 2873–2884 (2015).
34. M. A. German, S. Luo, G. Schroth, B. C. Meyers, P. J. Green, Construction of Parallel Analysis of RNA Ends (PARE) libraries for the study of cleaved miRNA targets and the RNA degradome. *Nat. Protoc.* **4**, 356–362 (2009).
35. Y. Harigaya, R. Parker, Global analysis of mRNA decay intermediates in Saccharomyces cerevisiae. *Proc. Natl. Acad. Sci. U.S.A.* **109**, 11764–11769 (2012).
36. S. Lykke-Andersen *et al.*, Human nonsense-mediated RNA decay initiates widely by endonucleolysis and targets snoRNA host genes. *Genes Dev.* **28**, 2498–2517 (2014).
37. S. A. Schmidt *et al.*, Identification of SMG6 cleavage sites and a preferred RNA cleavage motif by global analysis of endogenous NMD targets in human cells. *Nucleic Acids Res.* **43**, 309–323 (2015).
38. A. Lebreton, R. Tomecki, A. Dziembowski, B. Séraphin, Endonucleolytic RNA cleavage by a eukaryotic exosome. *Nature* **456**, 993–996 (2008).
39. D. Schaeffer *et al.*, The exosome contains domains with specific endoribonuclease, exoribonuclease and cytoplasmic mRNA decay activities. *Nat. Struct. Mol. Biol.* **16**, 56–62 (2009).
40. C. Schneider, E. Leung, J. Brown, D. Tollervey, The N-terminal PIN domain of the exosome subunit Rrp44 harbors endonuclease activity and tethers Rrp44 to the yeast core exosome. *Nucleic Acids Res.* **37**, 1127–1140 (2009).
41. S. K. Doamekpor, A. Gozdek, A. Kwasnik, J. Kufel, L. Tong, A novel 5′-hydroxyl dinucleotide hydrolase activity for the DXO/Rai1 family of enzymes. *Nucleic Acids Res.* **48**, 349–358 (2020).
42. M. J. Payea, A. C. Hauke, T. De Zoysa, E. M. Phizicky, Mutations in the anticodon stem of tRNA cause accumulation and Met22-dependent decay of pre-tRNA in yeast. *RNA* **26**, 29–43 (2020).

43. M. Oeffinger *et al*., Rrp17p is a eukaryotic exonuclease required for 5′ end processing of Pre-60S ribosomal RNA. *Mol. Cell* **36**, 768–781 (2009).
44. X.-C. Yang *et al*., Studies with recombinant U7 snRNP demonstrate that CPSF73 is both an endonuclease and a 5′–3′ exonuclase. *RNA* **26**, 1345–1359 (2020).
45. B. Tsanova, P. Spatrick, A. Jacobson, A. van Hoof, The RNA exosome affects iron response and sensitivity to oxidative stress. *RNA* **20**, 1057–1067 (2014).
46. S. Ben-Aroya *et al*., Toward a comprehensive temperature-sensitive mutant repository of the essential genes of Saccharomyces cerevisiae. *Mol. Cell* **30**, 248–258 (2008).
47. J. S. Anderson, R. P. Parker, The 3′ to 5′ degradation of yeast mRNAs is a general mechanism for mRNA turnover that requires the SKI2 DEVH box protein and 3′ to 5′ exonucleases of the exosome complex. *EMBO J.* **17**, 1497–1506 (1998).
48. D. Schaeffer, A. van Hoof, Different nuclease requirements for exosome-mediated degradation of normal and nonstop mRNAs. *Proc. Natl. Acad. Sci. U.S.A.* **108**, 2366–2371 (2011).
49. C. L. Peebles, R. C. Ogden, G. Knapp, J. Abelson, Splicing of yeast tRNA precursors: A two-stage reaction. *Cell* **18**, 27–35 (1979).
50. C. L. Greer, C. L. Peebles, P. Gegenheimer, J. Abelson, Mechanism of action of a yeast RNA ligase in tRNA splicing. *Cell* **32**, 537–546 (1983).
51. A. Kumar *et al*., Subcellular localization of the yeast proteome. *Genes Dev.* **16**, 707–719 (2002).
52. W.-K. Huh *et al*., Global analysis of protein localization in budding yeast. *Nature* **425**, 686–691 (2003).
53. B. Dubreuil *et al*., YeastRGB: Comparing the abundance and localization of yeast proteins across cells and libraries. *Nucleic Acids Res.* **47**, D1245–D1249 (2019).
54. K. Chatterjee, R. T. Nostramo, Y. Wan, A. K. Hopper, tRNA dynamics between the nucleus, cytoplasm and mitochondrial surface: Location, location, location. *Biochim. Biophys. Acta. Gene Regul. Mech.* **1861**, 373–386 (2018).
55. V. M. Reyes, J. Abelson, Substrate recognition and splice site determination in yeast tRNA splicing. *Cell* **55**, 719–730 (1988).
56. S. Fabbri *et al*., Conservation of substrate recognition mechanisms by tRNA splicing endonucleases. *Science* **280**, 284–286 (1998).
57. C. L. Greer, D. Söll, I. Willis, Substrate recognition and identification of splice sites by the tRNA-splicing endonuclease and ligase from Saccharomyces cerevisiae. *Mol. Cell. Biol.* **7**, 76–84 (1987).
58. M. I. Baldi, E. Mattoccia, E. Bufardeci, S. Fabbri, G. P. Tocchini-Valentini, Participation of the intron in the reaction catalyzed by the Xenopus tRNA splicing endonuclease. *Science* **255**, 1404–1408 (1992).
59. C. L. Peebles, P. Gegenheimer, J. Abelson, Precise excision of intervening sequences from precursor tRNAs by a membrane-associated yeast endonuclease. *Cell* **32**, 525–536 (1983).
60. Y. Wan, A. K. Hopper, From powerhouse to processing plant: Conserved roles of mitochondrial outer membrane proteins in tRNA splicing. *Genes Dev.* **32**, 1309–1314 (2018).
61. S. Yoshinari *et al*., Archaeal pre-mRNA splicing: A connection to hetero-oligomeric splicing endonuclease. *Biochem. Biophys. Res. Commun.* **346**, 1024–1032 (2006).
62. S. V. Paushkin, M. Patel, B. S. Furia, S. W. Peltz, C. R. Trotta, Identification of a human endonuclease complex reveals a link between tRNA splicing and pre-mRNA 3′ end formation. *Cell* **117**, 311–321 (2004).
63. S. E. Peach, K. York, J. R. Hesselberth, Global analysis of RNA cleavage by 5′-hydroxyl RNA sequencing. *Nucleic Acids Res.* **43**, e108 (2015).
64. P. D. Cherry, S. E. Peach, J. R. Hesselberth, Multiple decay events target HAC1 mRNA during splicing to regulate the unfolded protein response. *eLife* **8**, e42262 (2019).
65. A. Ramirez, S. Shuman, B. Schwer, Human RNA 5′-kinase (hClp1) can function as a tRNA splicing enzyme in vivo. *RNA* **14**, 1737–1745 (2008).
66. J. Popow *et al*., HSPC117 is the essential subunit of a human tRNA splicing ligase complex. *Science* **331**, 760–764 (2011).
67. E. Karaca *et al*.; Baylor Hopkins Center for Mendelian Genomics, Human CLP1 mutations alter tRNA biogenesis, affecting both peripheral and central nervous system function. *Cell* **157**, 636–650 (2014).
68. A. E. Schaffer *et al*., CLP1 founder mutation links tRNA splicing and maturation to cerebellar development and neurodegeneration. *Cell* **157**, 651–663 (2014).
69. B. S. Budde *et al*., tRNA splicing endonuclease mutations cause pontocerebellar hypoplasia. *Nat. Genet.* **40**, 1113–1118 (2008).
70. K. Makanae, R. Kintaka, T. Makino, H. Kitano, H. Moriya, Identification of dosage-sensitive genes in Saccharomyces cerevisiae using the genetic tug-of-war method. *Genome Res.* **23**, 300–311 (2013).
71. E. Bufardeci, S. Fabbri, M. I. Baldi, E. Mattoccia, G. P. Tocchini-Valentini, In vitro genetic analysis of the structural features of the pre-tRNA required for determination of the 3′ splice site in the intron excision reaction. *EMBO J.* **12**, 4697–4704 (1993).
72. P. Fruscoloni, M. I. Baldi, G. P. Tocchini-Valentini, Cleavage of non-tRNA substrates by eukaryal tRNA splicing endonucleases. *EMBO Rep.* **2**, 217–221 (2001).
73. T. Yoshihisa, Handling tRNA introns, archaeal way and eukaryotic way. *Front. Genet.* **5**, 213 (2014).
74. A. Golani-Armon, Y. Arava, Localization of nuclear-encoded mRNAs to mitochondria outer surface. *Biochemistry (Mosc.)* **81**, 1038–1043 (2016).
75. N. Gadir, L. Haim-Vilmovsky, J. Kraut-Cohen, J. E. Gerst, Localization of mRNAs coding for mitochondrial proteins in the yeast Saccharomyces cerevisiae. *RNA* **17**, 1551–1565 (2011).
76. E. Eliyahu *et al*., Tom20 mediates localization of mRNAs to mitochondria in a translation-dependent manner. *Mol. Cell. Biol.* **30**, 284–294 (2010).
77. S. Xue, K. Calvin, H. Li, RNA recognition and cleavage by a splicing endonuclease. *Science* **312**, 906–910 (2006).
78. F. He, N. Amrani, M. J. O. Johansson, A. Jacobson, Chapter 6. Qualitative and quantitative assessment of the activity of the yeast nonsense-mediated mRNA decay pathway. *Methods Enzymol.* **449**, 127–147 (2008).
79. V. K. Nagarajan, P. M. Kukulich, B. von Hagel, P. J. Green, RNA degradomes reveal substrates and importance for dark and nitrogen stress responses of Arabidopsis XRN4. *Nucleic Acids Res.* **47**, 9216–9230 (2019).
80. J. Wu, A. K. Hopper, Healing for destruction: tRNA intron degradation in yeast is a two-step cytoplasmic process catalyzed by tRNA ligase Rlg1 and 5′-to-3′ exonuclease Xrn1. *Genes Dev.* **28**, 1556–1561 (2014).
81. J. E. Hurtig, V. K. Nagarajan, A. van Hoof, PARE of sen2 and rrp44 endonucleases. National Center for Biotechnology Information SRA. http://www.ncbi.nlm.nih.gov/sra/?term=PRJNA663967. Deposited 18 September 2020.